Published in final edited form as:
Anal Chem. 2011 March 15; 83(6): 2020–2028. doi:10.1021/ac2001737.

Generating Non-Linear Concentration Gradients in Microfluidic Devices for Cell Studies

Šeila Selimović[a], **Woo Young Sim**[a], **Sang Bok Kim**[a], **Yun Ho Jang**[a], **Won Gu Lee**[a,c], **Masoud Khabiry**[a], **Hojae Bae**[a], **Sachin Jambovane**[b], **Jong Wook Hong**[b,*], and **Ali Khademhosseini**[a,*]

[a] Center for Biomedical Engineering, Department of Medicine, Brigham & Women's Hospital, Harvard Medical School , Boston, 02115 and Harvard-MIT Division of Health Sciences and Technology, Massachusetts Institute of Technology, Cambridge, MA 02139, USA

[b] Department of Mechanical Engineering, Auburn University, 275 Wilmore Lab, Auburn, AL 36849

[c] Department of Mechanical Engineering, College of Engineering, Kyung Hee University, 1 Seochon, Giheung, Yongin, Gyeonggi 446-701, Republic of Korea

[d] Wyss Institute for Biologically Inspired Engineering, Harvard University, Boston, MA 02139, USA

Abstract

We describe a microfluidic device for generating non-linear (exponential and sigmoidal) concentration gradients, coupled with a microwell array for cell storage and analysis. The device has two inputs for co-flowing multiple aqueous solutions, a main co-flow channel and an asymmetrical grid of fluidic channels that allows the two solutions to combine at intersection points without fully mixing. Due to this asymmetry and diffusion of the two species in the co-flow channel, varying amounts of the two solutions enter each fluidic path. This induces exponential and sigmoidal concentration gradients at low and high flow rates, respectively, making the microfluidic device versatile. A key feature of this design is that it is space-saving, as it does not require multiplexing or a separate array of mixing channels. Furthermore, the gradient structure can be utilized in concert with cell experiments, to expose cells captured in microwells to various concentrations of soluble factors. We demonstrate the utility of this design to assess the viability of fibroblast cells in response to a range of hydrogen peroxide (H_2O_2) concentrations.

Keywords

Microfluidics; cell screening; concentration gradient

INTRODUCTION

Microscale technologies have proved to be a powerful tool for minimizing reagent volumes and reaction times in many biological and chemical applications.[1] Microfluidic methods are

*A. Khademhosseini: alik@rics.bwh.harvard.edu; J.W. Hong: jwhong@eng.auburn.edu.

AUTHOR CONTRIBUTIONS

ŠS, WYS, WGL, JW and AK designed the study. YHJ, SBK, WYS, MK, and ŠS fabricated the devices. ŠS, WYS, YHJ, and SBK conducted experiments, SBK conducted computer simulations. ŠS and SBK analyzed the data. ŠS, HJB, WYS, SBK, WGL, JWH and AK wrote the paper. All authors edited the manuscript. S and WYS contributed equally as first authors.

SUPPORTING INFORMATION AVAILABLE Selimovic_Gradient_AnalChem_SI_1.pdf

particularly well compatible with biological materials such as proteins and cells and allow researchers to precisely control the cellular environment in culture and to miniaturize assays for high-throughput applications. This is especially true for device materials[2, 3] such as poly(dimethylsiloxane) (PDMS) and room temperature vulcanizing (RTV) silicones, which are commonly used to fabricate active and passive fluidic channels and storage-reaction chambers. Standard applications include protein crystallization[4–6], nanoliter-volume PCR[7], microfabricated fluorescence activated cell sorting (uFACS)[8, 9], single-cell enzyme screening[10] and cell-based screening applications [11–14].

In the context of biological analysis, generation of (non-linear) chemical gradients and efficient mixing of the components within the integrated system is crucial for testing and analyzing biological responses to different analyte concentration levels[15–18]. The native microenvironment across cell membranes[19, 20] and for cellular responses during growth, differentiation and proliferation[21], for example, rarely includes linear concentration gradients. This has been shown in various cell studies including chemotaxis of breast cancer cells[22] that could not be induced by linear concentration gradient of the epidermal growth factor (EGF). Nonlinear gradients of EGF, however, showed marked chemotaxis of breast cancer cells. The role of non-linear[23], mainly exponential concentration gradients has also been studied in the context of cell proliferation[24], and ligand binding[25], and other cellular responses[26]. Hence, a platform that can generate nonlinear concentration gradients, and specifically exponential gradients, is required.

The reliability of these concentration gradients directly determines the experimental outcome.[27, 28] Concentration gradients for biological and chemical applications can be generated by diffusion, convection, and by adjusting the resistance of fluidic channels.[8, 28–30] A fundamental challenge in generating gradient profiles in microfluidic devices, in particular non-linear gradients, is establishing good spatial and temporal control over multi-component laminar flows with different solute concentrations. At the same time, it is desirable to maintain a small device footprint, to avoid external elements such as pressure controllers and eliminate fluidic channels solely dedicated to gradient generation, for example on-chip mixers and multiplexers. The need for handling such individual or multiple gradients has enabled the development of large-scale integrated microfluidic devices[10, 31], resulting in computer-controlled, programmable chips capable of parallel analysis and high-throughput screening of optimal experimental conditions[32–34]. In particular, acquiring the ability to rapidly and reliably generate concentration gradients in simple device structures may provide a useful tool in screening the complexity of biological microenvironment for stem cell and tissue engineering research[1, 35–37]. In this paper we describe a robust microfluidic design for creating nonlinear (exponential and sigmoidal) concentration gradients in high-throughput, well-containing microfluidic networks for biological analysis. Furthermore, we demonstrate the capabilities of the device for cell based experimentation.

Popular microfluidic gradient designs include the tree-like structure, originally developed by Jeon et al[28], the discrete gradient achieved by mixing of solutions via a multiplexer and mixer[10], and nonlinear gradient structures like the logarithmic structure described by Kim et al[8]. Both the tree-like and multiplexer designs include a series of fluidic channels dedicated to gradient formation, which minimizes the space available for analyte storage. Our device structure, in contrast, requires little space, as it does not rely on dedicated mixing channels, and only a single dual-port syringe pump as external support, such that the majority of the chip space can be used for performing experiments. The simplicity of this device contributes to its robustness, as there are virtually no microfluidic elements that can fail. Furthermore, unlike the logarithmic design, our device can generate multiple non-linear gradients. In our structure, two fluids containing different concentrations of various chemicals are injected into the main fluidic channel separately, via a single syringe pump. The fluid branches off

into several side channels that lead to an asymmetrical channel grid, which serves as a storage region. The grid feeds 512 storage wells placed in regular intervals along the branches (Figure 1a), so that the wells are filled with different mixtures of the two aqueous streams. As the solutions reach the side channels branching from the inlet channel, more and more of the main flow is removed, such that the interface between the two solutions inside the main channel repositions toward the grid (Figure 1b,c). For example, one branch may contain 90% clear solution and only 10% dye, and another branch may contain 50% clear solution and 50% dye etc. These mixtures then feed directly into the storage wells. In other words, when the two co-flowing streams reach the first branch, the total flow in the main channel is reduced, leading to a redistribution of the aqueous streams inside the channel. Therefore, if the ratio of the input flow rates is 1:1 inside the co-flow channel, and the first branch carries for example 25% of the total flow, then the ratio of the two solutions after this branch will change to 1:2. However, the total flow rate along all flow paths from the input to the exit (i.e. along any branch) is equal, as the path length and therefore resistance is constant (Figure 1e). More specifically, in the inlet or gradient generation region, the asymmetric channel geometry and the specific position of each branch combined with diffusion in the main channel lead to the formation of a one-dimensional concentration gradient in the side branches. An example is shown in the fluorescence image in Figure 1b. The corresponding data (dye concentration profiles measured along the red lines in Figure 1b) is plotted in Figure 1c.

A similar design for generating concentration gradients was developed by Holden et al.[38] In their work, the two aqueous solutions were co-flowed at low flow rates (up to 30 μl/hr) to induce mixing via diffusion as they were distributed into an array of narrow channels (without subsequent redistribution of flows inside the main channel), such that each channel carried a solution of a different final concentration. Our gradient generator is also based on this principle, with some differences in the geometrical features of the design. Furthermore, the gradient generator is merged with a microwell array that enables the use of the generated concentration gradients for performing high throughput cell studies. In addition, Holden et al[38] sampled a different experimental range, in that their flow rates were one to two orders of magnitude smaller, which enhanced mixing via diffusion and thus resulted in non-linear concentration gradients with different fit parameters.

As stated above, the main driving factor in our device is diffusion of the two aqueous solutions. In this paper we characterize the gradient generator by modifying this diffusion effect in two ways: a) by controlling the flow rates and b) using species of different diffusion constants. Finally, we demonstrate the usefulness of the device in analyzing cell viability upon exposure to various concentrations of a toxin.

EXPERIMENTAL SECTION

Gradient formation

The microfluidic device consists of two PDMS (Sylgard 184, Dow Corning) layers and is fabricated according to a standard soft lithography protocol (ESI). A schematic of the device structure is shown in Figure 1a. Two input channels are provided for the two solutions to be mixed; the solutions then combine and co-flow in a main fluidic channel (200 μm wide and 15 μm tall) before they enter the channel grid and subsequently fill the storage wells. The storage region houses 512 circular wells (200 μm height, 150 μm radius), placed at 800 μm intervals along a branch and at 1600 μm and 2200 μm intervals in the direction of the main flow, and it occupies an area of 1.25 cm × 1.1 cm. Grid channels are 100 μm wide and 15 μm deep with a rounded profile. There are 40 channels that branch off the inlet channel. In our experiments and simulations, however, we gather our measurements from wells placed along sixteen of these branches that are 2*d* and 2.75*d* apart, as the storage wells are

ultimately the feature of the device we are most interested in. From here on, we number these channels sequentially from 1 to 16 (where 1 is closest to the input and 16 is closest to the output). We note that in this version of the device the storage wells are connected not only via the long side branches, but also via short, perpendicular channels (1*d* in length). These channels are currently passive, i.e. they are not actively used and do not contribute to the gradient generation. They are designed, however, to serve as part of a future perfusion system that will allow for long-term cell culture.

To establish an exponential concentration gradient we rely on a volume-driven system (dual Harvard PhD 2000 syringe pump). We demonstrated the repeatability of the device and tested the effect of different input flow rates by using clear PBS solution and fluorescein sodium dye (Aldrich) solution (1 mg/ml in PBS, phosphate buffered saline, Invitrogen) as the two co-flowing aqueous solutions. The flow rates of both aqueous streams were equal in all experiments. Fluorescence images were collected on a microscope (Nikon TE2000-U, 2x achromat objective) and analyzed by using ImageJ software (rsbweb.nih.gov). The device was primed by filling it completely with PBS solution prior to the introduction of the dye. In all experiments, the clear solution entered the device through the input on the left (close to the channel grid) and the fluorescent dye was pumped through the opposite input (far from the channel grid). To study the fluid flow rates and stability, the width of each aqueous stream in the input channel was visualized for least one hour. When studying the effect of the flow rate on the resulting concentration gradient, we applied equal flow rates of 10, 50, 100 and 200 μl/hr to both aqueous streams. In assessing the reproducibility of the experiments, we conducted each experiment three times. The time to generate and stabilize the gradient was longest at 10 μl/hr (10 minutes) and shorter at higher flow rates. We measured the intensity of the fluorescence signal in each well and normalized it by comparing it to the fluorescence at the input channel (100% fluorescent dye solution), then averaged our results from the three sets of experiments. Last, we fit an exponential or sigmoidal curve to each averaged data set and determined the function parameters using the Microcal Origin plotting and data analysis software.

We also studied the effect of diffusion constant on the resulting concentration gradient. We compared the fluorescein sodium dye experiment at 100 μl/hr/stream with concentration gradients of two fluorescently labelled Dextran compounds, FITC-Dextran 10kDa (Sigma) and FITC-Dextran 70kDa (Sigma).

Numerical calculation

To support our experimental data we performed a full scale simulation of our experimental setup. This is a 2D simulation in the x–y plane. Since the gradient generation is independent of time (aside from a short stabilization period), the governing equations can be written as follows:

$$(\vec{u} \cdot \nabla)\vec{u} = -\nabla p + \frac{1}{Re}\nabla^2\vec{u} \tag{1}$$

$$\vec{u} \cdot \nabla\varphi = \frac{1}{Pe}\nabla^2\varphi \tag{2}$$

$$\nabla \cdot \vec{u} = 0, \tag{3}$$

where $u\rightarrow$ is the velocity vector, p is pressure, φ is analyte concentration density, *Re* and *Pe* represent Reynolds and Peclet numbers, respectively. Main parameters are *d*, the characteristic length (width of the main co-flow channel, 100 μm), *v*, kinematic viscosity of the suspension medium (10^{-6} m^2/s for water at room temperature) and *D*, mass diffusivity of the analyte ($4.9 \cdot 10^{-10}$ m^2/s for fluorescein sodium dye[39]). Another factor is *U*, the average velocity in the main flow channel (used in the simulation as reference velocity). For 10 μl/hr (and fluorescein sodium dye), $U = 0.000926$ m/s; for 50 μl/hr, $U = 0.00463$ m/s; for 100 μl/hr, $U = 0.00926$ m/s; and for 200 μl/hr, $U = 0.0185$ m/s. The other diffusion constants are on the order of $2.9 \cdot 10^{-11}$ m^2/s for FITC-Dextran 10kDa[40] and $2.3 \cdot 10^{-11}$ m^2/s for FITC-Dextran 70kDa[41].

The flow field of our device was determined by solving steady-state Navier-Stokes equations with the continuity equations expressed in Eq. (1) and (3). Analyte concentration was obtained by solving the convection-diffusion equation as shown in Eq. (2). In the flow field calculation, fixed velocity (see above) and pressure conditions were imposed at the inlet and outlet, respectively. To find the analyte concentration, the normalized concentration φ was set to 1 at the dye inlet and 0 at the clear solution inlet. At the outlet we used the Neumann boundary condition, that is the normal derivative of the concentration was set to 0. To evaluate the concentration distribution, a commercial solver (CFD-ACE+) was employed. The device geometry and dimensions used in the numerical calculation replicate precisely the experimental conditions.

The applied boundary conditions are as follows:

1. Inlet boundary condition

$$u_{n1}=u_0$$
$$u_{n2}=u_0$$
$$\varphi_1=0$$
$$\varphi_2=1$$

where u_{n1} and u_{n2} are magnitude of the normal velocities at inlet 1 and 2, respectively. u_0 is equal to Q/A, where Q is flow rate and A is channel cross section area. φ_1 and φ_2 are normalized analyte concentration at inlet 1 and 2, respectively. These inlet boundary conditions show that the analyte is introduced only through inlet 2 and analyte-free, clear solution is introduced through inlet 1.

2. Wall boundary condition

$$\mathbf{u}=\mathbf{0}$$
$$D\frac{\partial\varphi}{\partial n}\Big|_{wall}=0$$

where $\frac{\partial}{\partial n}n$ is the normal derivative and u is the velocity vector. We imposed a no-slip boundary condition for the flow velocity field and the zero normal derivative condition for the analyte concentration (Neumann boundary condition), that is, the normal derivative of the analyte concentration at the wall is set to zero. The analyte flux N can be written as

$$\mathbf{N}=\varphi\mathbf{u}-D\nabla\varphi$$

and the normal flux of the analyte at the wall can be expressed as

$$\mathbf{n}\cdot\mathbf{N}=\varphi\mathbf{u}\cdot\mathbf{n}-\mathbf{n}\cdot D\nabla\varphi=0 \quad \left(\because \mathbf{u}=\mathbf{0}, n\cdot D\nabla\phi=D\frac{\partial\phi}{\partial n}=0\right)$$

where N is the analyte flux vector and n is the unit normal vector at the wall. Therefore, normal flux of analyte at the wall is zero, that is, a zero flux boundary condition is imposed.

3. Outlet boundary condition

$$P_{static}=0$$
$$D\frac{\partial\varphi}{\partial n}\Big|_{outlet}=0$$

We imposed a constant pressure condition for the flow field and zero normal derivative of analyte concentration at the outlet (Neumann boundary condition). At the outlet, however, the normal flux of the analyte can be expressed as

$$\mathbf{n}\cdot\mathbf{N}=\varphi\mathbf{u}\cdot\mathbf{n}-\mathbf{n}\cdot D\nabla\varphi=\varphi\mathbf{u}\cdot\mathbf{n} \quad \left(\because n\cdot D\nabla\phi=D\frac{\partial\phi}{\partial n}=0\right)$$

that is, a convective normal flux condition was imposed.

Cell culture and cytotoxicity test

Cell experiments were conducted on NIH-3T3 mouse fibroblasts cultured in high glucose-Dulbecco's Modified Eagle Medium (DMEM, Gibco, USA) with 10% fetal bovine serum (FBS, Gibco, USA), 1% penicillin/streptomycin (Gibco, USA). Cells were grown in a humidified incubator at 37° C and supplemented with 5% CO_2 for 3 days, then trypsinized with 0.25% trypsin-EDTA (Gibco, USA) and harvested. Finally, cells were resuspended in 1 ml medium after centrifuging.

To sterilize the device, we pumped a 70% ethanol solution through the channels for 1 hour, then rinsed it with phosphate buffered saline (PBS, Invitrogen, USA) for three hours and finally filled the device completely with culture medium. The temperature of 37° C was maintained for the duration of the experiment. Cells were loaded into the device at a concentration of 2×10^6 cells/ml using a hand-held 1 ml plastic syringe (Becton-Dickinson). Once the cells were stored in wells at a low density (up to 50 cells per well), resulting in a monolayer of cells at the bottom of each well, a concentration gradient (at 50 μl/hr per stream) between 10 mM hydrogen peroxide (H_2O_2) solution with DMEM and pure PBS was established as described above and maintained for 60 minutes at constant flow. Hydrogen peroxide is known to affect the viability of various cell types, and at high concentrations can lead to necrosis in 3T3 cells.[42–44] After 60 minutes we gently disconnected the tubing containing hydrogel peroxide and PBS from the device to avoid disturbing the cells and plugged one of these two holes with a melted piece of tubing. There was no washing step. To determine the viability of 3T3 cells exposed to the gradient, we immediately stained the cells for 15 minutes inside the incubator with the Live/Dead Viability/Cytotoxicity Kit (Invitrogen, USA), calcein AM for live cells and ethidium homodimer (EthD-1) for dead cells. The excitation/emission wavelengths for calcein and ethidium homodimer are 494/517 nm and 528/617 nm, respectively. We introduced the kit using a hand-held Becton-Dickinson plastic syringe and then waited 15 minutes for the cells to be stained. We obtained fluorescence images of the cells (4x objective), in which red fluorescence indicates

dead cells, while green fluorescence indicates live cells. We counted the number of red and green fluorescent cells in all occupied wells on each side channel, normalized it against the total number of cells and calculated the average fraction of dead and live cells. In a control experiment cells were immersed in PBS and loaded into the device. Their viability was recorded immediately after loading. The details of the experiment were the same as described above, except that no hydrogen peroxide was used.

Results and Discussion

Gradient formation

Following the procedure described above we formed a concentration gradient of fluorescent dye on-chip. We observed a one-dimensional non-linear gradient of dye concentration across the device parallel to the main flow channel (Figure 2). We also observed a shallow concentration gradient along each branch, that is, normal to the main flow channel, but the difference between the lowest and highest concentration value in a branch was on average 0.05 and decreased with increasing flow rate. This variation may be due to the short orthogonally placed channels within the grid that connect two wells and that were originally designed for cell perfusion purposes, as described above (Figure 1a). In addition, we conducted all experiments three times (n=3) and plot here the averages of those measurements. The three concentration measurements differ from each other by at most 5%, which we contribute to experimental error (intrinsic variability in the flow rate applied by the syringe pump). Since we are interested in non-linear concentration gradients, a 5% difference in concentration measurement is acceptable, thus we consider our results robust and reproducible within our range of interest.

In both the experimental and simulation results (Figure 2), the higher the input flow rates, the steeper the initial slope of the exponential fit curve. This is because at high flow rates the two aqueous streams did not have sufficient time to mix completely via diffusion before the flow branches off into the side channels. Similarly, the maximum concentration of dye in channels close to the output (branch number 16) was proportional to the flow rate. At low flow rates, for example, the two streams were mixed well before they reached the last side channel, such that this last branch did not contain pure dye, but rather a mixture of clear solution and dye (e.g. 70% dye concentration and 30% clear solution). In contrast, at high flow rates, the two solutions did not mix significantly by the time they reached the last branch (well number 16), such that almost pure dye (95%) flowed through that branch.

This led to a special case at high flow rates (200 μl/hr per stream). Here, the concentration of dye did not increase exponentially, but approximated a sigmoidal curve in which branches 1–4 contained almost the same amount of dye. Branches 15 and 16 (and in some cases, branches 12 to 16) also had equal, albeit much higher dye concentrations. In branches 5–14 (or 5–11) the concentration of dye appeared to increase linearly (Figure 2b). A similar behavior was also evident in the simulation results (Figure 2c). Because of the large width of the linear region, this device has the potential to be used not only for generation of exponential and sigmoidal, but may also be used to generate linear concentration gradients. This observation can be explained by considering the extreme case, an extremely fast flow rate, in which the effect of diffusion is negligible. In this case the two solutions would flow much faster than they could mix via diffusion, such that the concentration gradient would be a sigmoidal function with a large slope, approximating a step function.

The effect of diffusion constant on the gradient generation is shown in Figure 3. Our experiments showed that as expected, the larger the radius and thus the molecular weight of the diffusing species, the slower the mixing via diffusion, and thus the steeper the initial

slope of the exponential concentration gradient. We fit two types of non-linear curves to the experimental data: An exponential curve of the form

$$y=y_0+Ae^{(-x/B)}$$

was fit to low flow rate data (10, 50, and 100 μl/hr/stream), and a sigmoidal Boltzman function,

$$y=\left[A_1-A_2/(1+e^{(x-x_0)/dx})\right]+A_2$$

was fit to high flow rate data (200 μl/hr/stream) collected from fluorescein sodium salt solution. (In case of FITC-Dextran solutions, most fits were sigmoidal.) In both equations the variable *x* indicates the branch number. The goodness of fit was determined visually – the low flow rate data (below 200 μl/hr/stream) is approximated better with an exponential decay curve, and high flow rate data is approximated better with a sigmoidal Boltzmann curve. Supplementary Table S1a contains the exponential fit parameters for experiments conducted with clear PBS solution and fluorescein sodium salt at flow rates ranging from 10 μl/hr to 200 μl/hr per stream and for the corresponding numerical simulations. The numerical results match our experimental results qualitatively, and the characteristic exponential and sigmoidal fit parameters are also comparable. Supplementary Table S1b contains the exponential fit parameters for experiments comparing the effect of different diffusion constants. Interestingly, there was a similarity between increasing the flow rate and lowering the diffusion constant. In both cases the defining parameter changed accordingly. In exponential fits to our experimental data, we view the initial slope *A* as the defining parameter that describes the concentration gradient: The higher the flow rate and the lower the diffusion constant, the larger *A*. With sigmoidal fits, we view the width of the saddle region *dx* as the defining factor: the higher the diffusion constant and the higher the flow rate, the smaller *dx* (see ESI, Table S1).

Cell culture and cytotoxicity test

In the cell experiment, we first seeded 3T3 fibroblast cells in the microwells. To achieve uniform cell seeding across all 512 storage wells in the device, the cells were introduced separately into each branch containing wells, by punching an additional input and an exit hole into each of those branches. The exit hole of any branch was only open during the cell loading at that particular branch. After cells were loaded into a particular branch, the respective access holes were plugged with melted tubing and not reopened, so that they did not affect the concentration gradient formation.

The seeded cells were on average 15 μm in diameter, roughly the same diameter as the channel height. The percentage of filled wells was measured to be ~ 93% with between 3 and 50 cells per well (the average number of cells per well was 12).

In most wells the cells were organized in a monolayer and not in clusters, allowing us to count them accurately using phase-contrast images. When in addition cell clusters were present we only counted the cells that were in focus at the bottom of the well, even if they were part of a cluster. After loading the cells, we established a H_2O_2 concentration gradient by simultaneously supplying PBS and hydrogen peroxide to the channel grid at 50 μl/hr for the duration of the experiment. We inspected the occupied wells visually before, during and after the introduction of the gradient and did not observe any movement of the cells which

had settled on the bottom of the 200 μm deep wells; these cells appeared to be undisturbed by the applied flow rate. Other cells, however, that had attached to the sides of the wells and were closer to the main flow channel were displaced by this flow. Forthcoming work from our laboratory analyzes the effect of shear and well depth on the stability of cell storage in this device.

The applied toxin gradient resulted in the highest fraction of dead cells in the top branch (1), and the highest fraction of live cells on the opposite end of the device (branch 16) (Figure 4a,b). Representative wells from each branch are shown in Figure 4b. We counted the number of dead (red) and live (green) cells in each well by using fluorescence images. Because of the large variation in the number of cells per well, we added the numbers of cells in sets of four wells each and treated those sets as individual populations, such that the number of cells in most sets varied between 20 and 70, with a statistically more reliable average number of 46. In other words, instead of 32 independent wells with an average of 12 cells we counted 8 sets of 4 wells each with an average of 46 cells. We normalized the number of live and dead cells in each set by comparing them to the total number of cells in that set to find the fraction of live and dead cells. The numbers were then averaged across the 8 sets on each branch and plotted (Figure 4c). The fraction of live cells increased non-linearly with branch number, confirming qualitatively our previous experimental and simulation results. Similarly, the fraction of dead cells decreased non-linearly with branch number.

We note that some cells fluoresced at both red and green wavelengths. Those cells were originally healthy, thus fluorescing green, but were damaged with prolonged exposure to the toxin, thus starting to fluoresce red. Whether we labelled these bi-signalling cells as live or dead, the resulting curves were always non-linear (exponential), but their fit parameters differed. As this group of cells was already damaged and was thus expected to die, we chose, however, to count them as dead cells.

The diffusion constant of hydrogen peroxide can be estimated at 10^{-9} m^2/s[45, 46] for a small molecule. We can infer from the 50 μl/hr data of FITC-300Da, which differs only by a factor of ½, that the H_2O_2 concentration at branch 16 should be 2.5mM. The percentage of dead cells at this branch is 40%. Literature values43 for a 20 minute long exposure to 2mM H_2O_2 indicate a 20% necrotic rate. As the cell death rate depends both on toxin concentration and exposure time, our observation is in accordance with the literature results.

In the control experiment, in which we counted the number of live and dead cells in all branches after loading and without the presence of toxin (Figure 4d), we treated each well separately, rather than in clusters. The average number of cells per well was 16. The result indicates that the viability is close to 100% in all branches. Also, the calculated maximum shear stress acting on a cell is 0.27 dyne cm^{-2} at 200 μl/hr[47] is not large enough to contribute to cell death, which is in agreement with literature results[48–51].

CONCLUSION

We developed a microfluidic device for generating exponential and sigmoidal concentration gradients by exploiting diffusion of two aqueous species in an asymmetrical design. The flow patterns of two miscible aqueous solutions generate concentration gradients parallel to the input line and were investigated with respect to the applied flow rates and diffusion constants of the two co-flowing solutions and species.

At low flow rates of water and fluorescent sodium dye (10, 50, and 100 μl/hr per stream) we observed exponential gradients with an increasingly steeper initial slope, which reached higher final concentrations with increasing flow rate. At a high flow rate (200 μl/hr per

stream), however, we observed sigmoidal concentration gradients. The saddle region of such gradients could be approximated with a linear curve, making this device useful for applications requiring linear concentration gradients. Further, an increasing flow rate was imitated by using species with smaller diffusion constants. These experimental parameters were equivalent insofar as they weakened the mixing of the two species, leading to a steeper initial slope of the concentration gradient. For fluorescently labeled Dextran, for example, the sigmoidal behavior sets on at a lower flow rate (50 μl/hr per stream). Lastly, we demonstrated the applicability of the device in biological studies, namely a live-dead assay on fibroblast cells. The resulting concentration gradients of live and dead cells were non-linear, as expected from our device characterization study.

The main advantage of the microfluidic device presented here is its small footprint, as it does not include a dedicated mixing region, and it is capable of producing specific concentration gradients of different biochemical components solely by controlling the applied flow rates. With regard to external equipment, operation of this device only requires a dual syringe pump, a standard equipment item in most biology laboratories. As such, this device essentially has no fallible elements, increasing its robustness. Our microfluidic device therefore has the potential to become a useful tool for studying the effects of microenvironments on biological activities, e.g. cell behavior in response to various natural or synthetic stimuli, from basic biological applications to drug discovery studies. Our future work will focus on improving our cell seeding capabilities in this PDMS device by utilizing the short cross-channels between individual wells and introducing microfluidic valves to control the fluid delivery. We plan to conduct further cell studies, for example subject stem cells to different growth factors or drug gradients. For example, we envision first conducting a screening experiment using a sigmoidal concentration gradient, then using these results focusing on a particular concentration range by applying an exponential gradient. We will also work on modifying the device design to allow for long-term cell culture, for example by introducing a media perfusion system. Apart from cell studies, future applications could include protein crystallization, where protein droplets instead of cells will be captured in the storage wells and subjected to different pH gradients.

Supplementary Material

Refer to Web version on PubMed Central for supplementary material.

Acknowledgments

This paper was supported by the National Institutes of Health (EB008392; HL092836; EB009196; DE019024), National Science Foundation (DMR0847287), the Institute for Soldier Nanotechnology, the Office of Naval Research, and the US Army Corps of Engineers. W. Y. Sim was partially supported by the Korea Research Foundation Grant funded by the Korean Government (KRF-2008-357-D00099). W. G. Lee was partially supported by the Basic Science Research Program through the National Research Foundation of Korea (NRF), funded by the Ministry of Education, Science and Technology (2010-0005219).

References

1. Khademhosseini A, Langer R, Borenstein J, Vacanti JP. Proc Natl Acad Sci U S A. 2006; 103:2480–2487. [PubMed: 16477028]
2. Ostuni E, Chen CS, Ingber DE, Whitesides GM. Langmuir. 2001; 17:2828–2834.
3. Xia Y, Whitesides GM. Angewandte Chemie International Edition. 1998; 37:550–575.
4. Selimović Š, Jia Y, Fraden S. Crystal Growth & Design. 2009; 9:1806–1810. [PubMed: 20161207]
5. Hansen CL, Skordalakes E, Berger JM, Quake SR. Proceedings of the National Academy of Sciences of the United States of America. 2002; 99:16531–16536. [PubMed: 12486223]
6. Selimović Š, Gobeaux F, Fraden S. Lab Chip. 2010

7. Liu J, Enzelberger M, Quake S. Electrophoresis. 2002; 23:1531–1536. [PubMed: 12116165]
8. Bang H, Chung C, Kim J, Kim S, Chung S, Park J, Lee W, Yun H, Lee J, Cho K, Han DC, Chang J. Microsystem Technologies. 2006; 12:746–753.
9. Baret JC, Miller OJ, Taly V, Ryckelynck M, El-Harrak A, Frenz L, Rick C, Samuels ML, Hutchison JB, Agresti JJ, Link DR, Weitz DA, Griffiths AD. Lab Chip. 2009; 9:1850–1858. [PubMed: 19532959]
10. Thorsen T, Maerkl SJ, Quake SR. Science. 2002; 298:580–584. [PubMed: 12351675]
11. Khademhosseini A, Jon S, Suh KY, Eng G, Yeh J, Tran TT, Langer R. Advanced Materials. 2003; 15:1995–2000.
12. Khademhosseini A, Burdick J, Langer R. Langmuir. 2004; 20:5153–5156. [PubMed: 15986641]
13. Khademhosseini A, Yeh J, Eng G, Kazi H, Borenstein JJK, Farokhzad J, Langer R. Lab on a Chip. 2005; 5:1380–1386. [PubMed: 16286969]
14. Chung BG, Kang L, Khademhosseini A. Expert Opin Drug Discov. 2007; 2:1–16.
15. Jain M, Young A, Nandakumar M. Biomicrofluidics. 2010; 4:014110, 014111–014113.
16. Fuller D, Chen W, Adler M, Groisman A, Levine H, Rappel WJ, Loomis WF. Proceedings of the National Academy of Sciences. 2010; 107:9656–9659.
17. Rosoff WJ, Urbach JS, Esrick MA, McAllister RG, Richards LJ, Goodhill GJ. Nat Neurosci. 2004; 7:678–682. [PubMed: 15162167]
18. Eichele G, Thaler C. Journal of Cell Biology. 1987; 105:1917–1923. [PubMed: 3667700]
19. Huckabee W. Journal of Applied Physiology. 1956; 9:163. [PubMed: 13376422]
20. Leaf A. Annals of the New York Academy of Sciences. 1959; 72:396–404. [PubMed: 13627925]
21. Hall, MRM.; Thomas, G. Cell growth: control of cell size. CSHL Press; 2004.
22. Wang S-JSW, Lin F, Minh-Canh Nguyen C, Li Jeon N. Experimental Cell Research. 2004:180–189. [PubMed: 15383325]
23. Li CW, Chen R, Yang M. Lab Chip. 2007; 7:1371–1373. [PubMed: 17896024]
24. Norrby K, Franzen L. Developmental Biology - Plant. 1980; 16:31–37.
25. Mountcastle DB, Freire E, Biltonen RL. Biopolymers. 1976; 15:355–371.
26. Saadi W, Wang SJ, Lin F, Jeon NL. Biomedical Microdevices. 2006; 8:109–118. [PubMed: 16688570]
27. Hao C, Jens-Christian M. Applied Physics Letters. 2004; 84:2193–2195.
28. Jeon NL, Dertinger SKW, Chiu DT, Choi IS, Stroock AD, Whitesides GM. Langmuir. 2000; 16:8311–8316.
29. Jiang X, Xu Q, Dertinger SKW, Stroock AD, Fu T-m, Whitesides GM. Analytical Chemistry. 2005; 77:2338–2347. [PubMed: 15828766]
30. Irimia D, Geba DA, Toner M. Analytical Chemistry. 2006; 78:3472–3477. [PubMed: 16689552]
31. Hong JW, Quake SR. Nat Biotechnol. 2003; 21:1179–1183. [PubMed: 14520403]
32. Gu W, Zhu X, Futai N, Cho BS, Takayama S. Proceedings of the National Academy of Sciences of the United States of America. 2004; 101:15861–15866. [PubMed: 15514025]
33. Hong JW, Studer V, Hang G, Anderson WF, Quake SR. Nature Biotechnology. 2004; 22:435–439.
34. Ottesen EA, Hong JW, Quake SR, Leadbetter JR. Science. 2006; 314:1464–1467. [PubMed: 17138901]
35. Khetani SR, Bhatia SN. Nature Biotechnology. 2008; 26:120–126.
36. Anderson DG, Levenberg S, Langer R. Nature Biotechnology. 2004; 22:863–866.
37. Hwang YS, Chung BG, Ortmann D, Hattori N, Moeller HC, Khademhosseini A. Proceedings of the National Academy of Sciences. 2009; 106:16978–16983.
38. Holden MA, Kumar S, Castellana ET, Beskok A, Cremer PS. Sensors and Actuators B: Chemical. 2003; 92:199–207.
39. Rani SA, Pitts B, Stewart PS. Antimicrob Agents Chemother. 2005; 49:728–732. [PubMed: 15673757]
40. Gregor T, Bialek W, de Ryuter van Steveninck RR, Tank DW, Wieschaus EF. PNAS. 2005; 102:18403–18407. [PubMed: 16352710]

41. Periasamy N, Verkman AS. Biophysics journal. 1998; 75:557–567.
42. DiPietrantonio AM, Hsieh T, Wu JM. Biochem Biophys Res Commun. 1999; 255:477–482. [PubMed: 10049734]
43. Barros LF, Kanaseki T, Sabirov R, Morishima S, Castro J, Bittner CX, Maeno E, Ando-Akatsuka Y, Okada Y. Cell Death Differ. 2003; 10:687–697. [PubMed: 12761577]
44. Arnold RS, Shi J, Murad E, Whalen AM, Sun CQ, Polavarapu R, Parthasarathy S, Petros JA, Lambeth JD. Proceedings of the National Academy of Sciences of the United States of America. 2001; 98:5550–5555. [PubMed: 11331784]
45. Peroxide, U.
46. Tang A, Sandall OC. J Chem Eng Data. 1985; 30:189–191.
47. Gaver DP, Kute SM. Biophysical Journal. 1998; 75:721–733. [PubMed: 9675174]
48. Khabiry M, Chung BG, Hancock MJ, Soundararajan HC, Du Y, Cropek DC, Lee WG, Khademhosseini A. Small. 2009; 5:1186–1194. [PubMed: 19242937]
49. Du Y, Hancock MJ, He Y, Villa-Uribe J, Wang B, Cropek D, Khademhosseini A. Biomaterials. 2010; 31:2686–2694. [PubMed: 20035990]
50. Du Y, Shim J, Vidula M, lo E, Chung BG, Hancock M, Borenstein MJ, Cropek D, Khademhosseini A. Lab Chip. 2009; 9
51. Truskey GA, Proulx TL. Biomaterials. 1993; 14:243–254. [PubMed: 7682850]

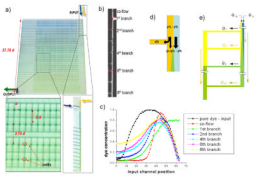

Figure 1.

a) Device structure with key dimensions (d = 800 μm). The input line for the two co-flowing solutions is shown on the right; several channels branch off and lead to the channel grid left of it. Magnified images show storage wells (placed at some intersections of the grid channels) and the gradient generation section (main input channel with side branches). Gradient generation region: b) Fluorescence photograph showing eight side branches. Note that the device has originally been designed with an additional exit channel for flushing out potential clogs near the inputs. This channel points to the right of the first branch and is permanently closed in our experiments. The white dashed line outlines the edge of the channel, with clear solution on the left and fluorescent dye on the right. The two solutions mix via diffusion as they travel through the main channel, such that different amounts of either solution enter the side branches, giving rise to a non-linear concentration gradient along the input flow direction. The red lines indicate positions along the input line where the concentration profile was measured. A graph of these concentration profiles is shown in c). d) Sketch showing a single side branch, illustrating the redistribution of flow in the main channel and e) sketch of the full device, showing that different flow paths (e.g. the yellow and the green path, labeled Q_2 and Q_{16}) have almost equal dimensions and therefore equal resistance. (Online in color.)

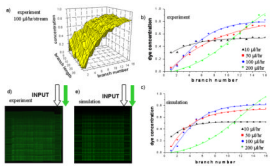

Figure 2.

a) 3D concentration profile of fluorescein sodium salt as a function of branch number and length, when introduced into the device together with a clear solution at 100 μl/hr per stream (data stems from a single experiment). b) Experimental data (symbols, averaged from three experiments) and corresponding exponential and sigmoidal fit curves (lines) for the co-flow of clear solution and a fluorescent dye solution. The listed flow rates are applied to each stream. For n=3 the standard deviation is below 9%, but we omit error bars to keep the graph readable. c) Corresponding simulation results. d) Stitched image of the microfluidic device at 50 μl/hr per stream and e) the corresponding simulation result. (Online in color.)

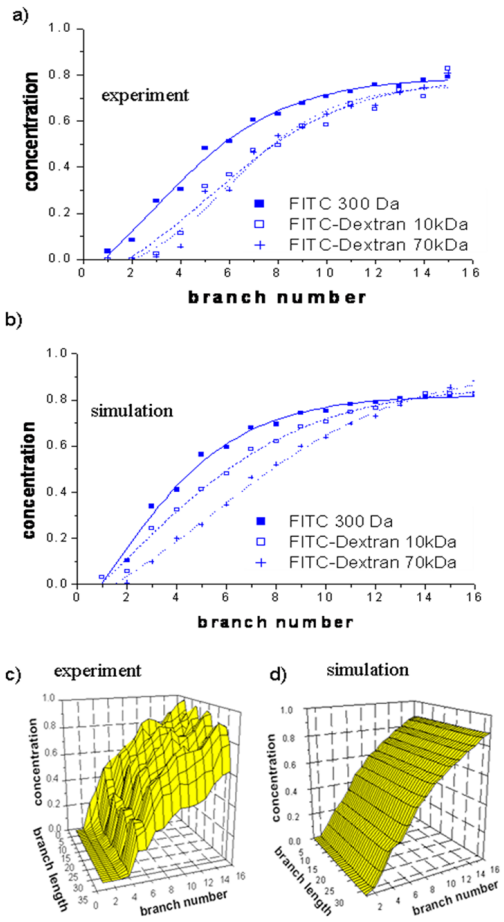

Figure 3.

Comparison of a) experimental (n=3) and b) simulation results for concentration gradients of three molecular species with different diffusion constants at 100 μl/hr/stream. The standard deviation in a) is below 9%, but we omit here the error bars to keep the graph readable. c) 3D representation of a single 100 μl/hr/stream experiment with FITC_Dextran 70kDa. Experiment and d) simulation. (Online in color.)

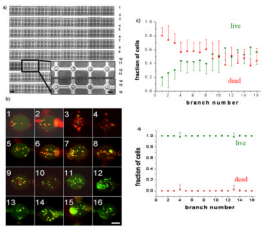

Figure 4.

Live-dead assay of 3T3 cells due to an exponential concentration gradient of H_2O_2. a) Stitched phase contrast photograph of the storage region with seeded cells (scale bar: 800 μm). Inset: typical wells (scale bar: 200 μm). b) Superposed red and green fluorescence images of cells stored in wells on branches 1 to 16, with decreasing H_2O_2 concentration (scale bar: 100 μm). c) Fraction of live and dead cells as a function of branch number, in response to the toxin gradient. d) Fraction of live and dead cells in the control experiment, immediately after loading and without the presence of hydrogen peroxide. The error bars in c) and d) are standard deviation values. For easier viewing, we only include one set of error bars for each data set.